

# High-efficiency shallow-etched grating on GaAs membranes for quantum photonic applications

Xiaoyan Zhou, Irina Kulkova, Toke Lund-Hansen, Sofie Lindskov Hansen, Peter Lodahl, and Leonardo Midolo

Citation: *Appl. Phys. Lett.* **113**, 251103 (2018); doi: 10.1063/1.5055622

View online: <https://doi.org/10.1063/1.5055622>

View Table of Contents: <http://aip.scitation.org/toc/apl/113/25>

Published by the [American Institute of Physics](#)

---

---



The image shows a silver, rack-mountable electronic instrument with a large color touchscreen. The screen displays four measurement panels: 'Continuity' (Not run), 'Contact Check' (2019-01-01 at 01:59, 2607 ms), 'Resistivity' (2019-01-01 at 01:59, 1008 ms), and 'FastHall™' (with a circular progress indicator). The instrument has a 'Measure Ready' indicator and 'M91 FastHall' branding on the front panel.

**Measure Ready**  
**M91 FastHall™ Controller**

A revolutionary new instrument  
for complete Hall analysis

 Lake Shore  
CRYOTRONICS

# High-efficiency shallow-etched grating on GaAs membranes for quantum photonic applications

Xiaoyan Zhou,<sup>1,a)</sup> Irina Kulkova,<sup>2</sup> Toke Lund-Hansen,<sup>2</sup> Sofie Lindskov Hansen,<sup>1</sup> Peter Lodahl,<sup>1</sup> and Leonardo Midolo<sup>1</sup>

<sup>1</sup>Center for Hybrid Quantum Networks (Hy-Q), University of Copenhagen, Blegdamsvej 17, 2100-DK Copenhagen, Denmark

<sup>2</sup>Sparrow Quantum, Blegdamsvej 17, 2100-DK Copenhagen, Denmark

(Received 8 September 2018; accepted 4 December 2018; published online 19 December 2018)

We have designed and fabricated a shallow-etched grating on gallium arsenide nanomembranes for efficient chip-to-fiber coupling in quantum photonic integrated circuits. Experimental results show that the grating provides a fiber-coupling efficiency of  $>60\%$ , a greatly suppressed back reflection of  $<1\%$  for the designed wavelength of 930 nm, and a 3-dB bandwidth of  $>43$  nm. Highly efficient single-photon collection from embedded indium arsenide quantum dots to an optical fiber was realized with the designed grating, showing an average six-fold increase in the photon count compared to commonly used circular gratings, offering an efficient interface for on-chip quantum information processing. *Published by AIP Publishing.* <https://doi.org/10.1063/1.5055622>

Quantum photonic integrated circuits are a promising approach to realizing scalable quantum information processing. Among various materials and platforms, the gallium arsenide (GaAs) material system stands out for offering indispensable quantum functionalities such as single-photon generation, manipulation, and detection, which could be entirely integrated in the same chip.<sup>1</sup> In particular, suspended GaAs nanomembranes have been successfully used to construct low-loss and high-performance devices,<sup>2,4</sup> including highly efficient on-demand single-photon sources with embedded indium arsenide (InAs) quantum dots (QDs)<sup>3–7</sup> and complex quantum photonic devices such as on-chip phase shifters, routers, and switches.<sup>8–11</sup>

Despite the blossoming of planar GaAs quantum technologies, efficient device characterization and single-photon extraction remain a challenge due to the lack of a reliable and reproducible method to couple light in and out of the chip. Both in-plane and out-of-plane approaches have been developed aiming at solving this issue. In-plane methods, such as end-fire inverted tapers, spot converters,<sup>3,12</sup> and evanescent microfiber couplers,<sup>13–15</sup> provide the highest coupling efficiencies; however, they are fabrication and alignment demanding. Vertical free-space approaches using on-chip gratings are instead easier to implement, are more convenient for cryostats having only optical access from a top window, and allow for quicker characterization of a large number of multi-port devices.

The most widely used out-coupling structure with QDs in suspended GaAs membranes is a circular grating (CG).<sup>3,9,16–18</sup> It is a second-order grating with a pitch of  $\lambda/(2n)$ , where  $\lambda$  is the free-space wavelength and  $n$  is the refractive index of the membrane. The grating induces destructive interference in the planar propagation direction, causing light to be scattered upwards to an objective lens. Such a grating can be fabricated and etched across the membrane with waveguides using a single lithographic step,<sup>2</sup> but the poor directionality and the non-Gaussian shape of the

out-scattered beam result in low coupling efficiency into optical fibers. Moreover, the strong back-reflection of a circular grating adds unwanted Fabry-Pérot (FP) resonances that ultimately degrade the device performance<sup>17</sup> and make the characterization of an integrated circuit (e.g., insertion loss measurements) largely inaccurate.

In silicon-on-insulator (SOI) photonics, surface focused grating couplers have been developed and optimized for moderately high coupling efficiency (above 50%), large bandwidth, low back-reflection, high polarization selectivity, and a sufficient fiber alignment tolerance.<sup>19</sup> These results, obtained by optimizing diffractive gratings over more than a decade in the mature SOI platform, suggest that much can be gained by adapting these structures to the GaAs suspended platform.

In this work, we demonstrate a focusing grating coupler integrated with a suspended planar GaAs quantum circuit which includes semiconductor QDs as efficient single-photon sources. While gratings working at room temperature are typically characterized by direct fiber coupling,<sup>19</sup> we characterize our gratings in a cryostat with a micro-photoluminescence setup for efficient single-photon excitation,<sup>20</sup> where light is collected vertically through an objective and then sent into a standard single-mode fiber. Experimental results show significant improvement of the chip-to-fiber coupling efficiency to  $>60\%$  and greatly suppressed back-reflection to  $<1\%$  for the central working wavelength of 930 nm, in good agreement with numerical simulations. Single-photon collection efficiency shows an average six-fold increase compared to circular gratings fabricated on the same sample. These results make shallow-etched gratings (SEGs) suitable for characterizing advanced and sensitive quantum nanophotonic devices, in particular for non-linear transmission experiments<sup>7</sup> and insertion loss measurements.

A cross-section schematic of the focusing shallow-etched grating coupler is shown in Fig. 1(a). The waveguide mode propagating in the  $x$  direction is diffracted upwards by the grating, with an emission angle of  $\theta$  to the vertical

<sup>a)</sup>Author to whom correspondence should be addressed: xiaoyan.zhou@nbi.ku.dk

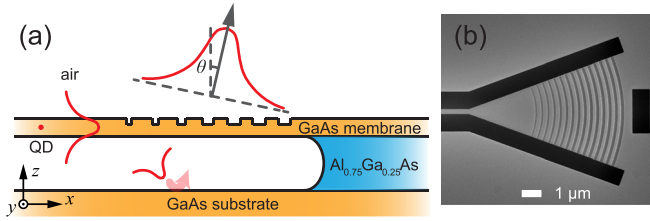


FIG. 1. (a) Schematic cross-section of the chirped shallow-etched grating couplers integrated with quantum photonic structures in a GaAs membrane platform. (b) Top-view scanning electron microscopy image of the device.

direction. The basic working principle of the grating can be described by the Bragg condition<sup>21</sup>

$$\beta - k_x = m \cdot \frac{2\pi}{\Lambda},$$

where  $\beta = 2\pi\bar{n}_{\text{eff}}/\lambda_0$  is the propagation constant of the membrane slab mode,  $k_x = 2\pi/\lambda_0 \cdot \sin \theta$  is the projected wavevector component of the diffracted light along the propagation direction,  $m$  is the order of diffraction, and  $\Lambda$  is the grating period.  $\bar{n}_{\text{eff}}$  is the average effective refractive index of the membrane. Here, we consider only the transverse-electric-like (TE-like) mode because the QDs are in the center of the GaAs membrane and the in-plane dipole moment only couples to the TE-like mode.<sup>22</sup> In the case of the aforementioned circular grating design,  $\Lambda$  is chosen so that  $\beta = 2\pi/\Lambda$ , resulting in the vertical scattering of the first-order diffraction ( $k_x = 0$ ) and the backward propagation of the second-order diffraction. To avoid back-reflection, a small emission angle ( $\theta$ ) is necessary. Using a fixed fill factor  $\text{FF} = 50\%$  and an etch depth  $\text{ED} = 50$  nm, our 160 nm GaAs membrane has an estimated  $\bar{n}_{\text{eff}} = 2.79$ . The working wavelength is chosen to be  $\lambda_0 = 930$  nm to match the QD emission wavelength. We design the emission angle  $\theta = 10^\circ$ , which gives a pitch  $\Lambda = \lambda_0/(\bar{n}_{\text{eff}} - \sin \theta) = 355$  nm.

To achieve high coupling efficiency, it is important to ensure constructive interference of the light reflected from the substrate and scattered upwards from the grating. The outgoing beam shape should also be optimized to match the fiber mode profile. For this purpose, we used commercially available finite difference time domain (FDTD) simulation software.<sup>23</sup> First, a uniform grating was optimized for maximum directionality and minimum back-reflection at a wavelength of 930 nm with a two-dimensional model. Using the theoretical parameters calculated above, an optimal sacrificial layer thickness of  $1.15 \mu\text{m}$  was found to give a maximum transmission of 68.8% and a reflection of 1.84%. Then, a full three-dimensional (3D) model of the apodized focusing grating was run to maximize the coupling into a single-mode fiber. We applied the apodization by inducing a linear reduction of the FF along the propagation direction. In fabricated devices, the ED decreases with the FF due to the loading effect in the reactive ion etching (RIE) process.<sup>24</sup> From the scanning electron micrographs, we find a relationship between the ED and the FF given by  $\text{ED} = (-6.59 \cdot \text{FF}^{-1.33} + 66.47)$  nm. The loading effect is taken into account in the numerical model.

Figure 2(a) shows the main electromagnetic field component of the TE-like mode, i.e.,  $E_y$ , in the cross-section of

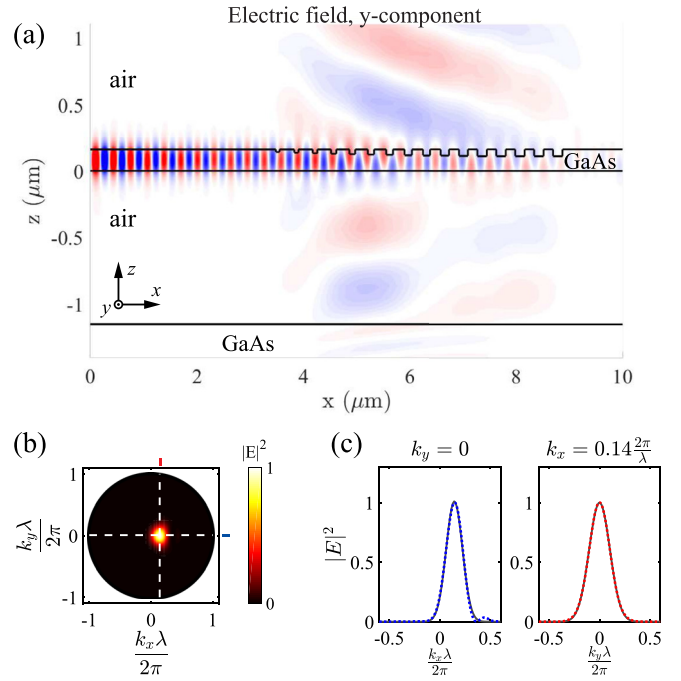


FIG. 2. (a) Cross-section of the 3D optical simulation showing that most of the light is scattered upward with an angle. (b) The far-field pattern of the grating emission. (c)  $x$ -cut (blue dotted line) and  $y$ -cut (red dotted line) of (b) with Gaussian fits shown by solid lines.

the grating. Most of the light is scattered upward with an emission angle  $\theta = 8.4^\circ$  for the designed wavelength of 930 nm. As shown by the far-field plots in Figs. 2(b) and 2(c), the outgoing beam has good directionality and a Gaussian beam profile with a small numerical aperture ( $\text{NA}_x = 0.16$ ,  $\text{NA}_y = 0.21$ ), facilitating free-space collection and coupling into fibers.

The wavelength-dependent transmission, reflection, and emission angle are shown in Fig. 3. At the design wavelength of 930 nm, the power scattered toward the objective is 76.1%, while the transmission into the fiber reaches 74.6% with a mode overlap of 98%. With a fixed collection angle, the grating has a 3-dB transmission bandwidth of 57 nm. By changing the collection angle, one can optimize the transmission for other wavelengths, e.g., 910 nm [shown in Fig. 3(a)], which gives similar efficiency and bandwidth as the transmission features for 930 nm. We note that the drop in transmission away from the designed wavelength is mainly due to the change in the emission angle from the grating. Using an objective with sufficient numerical aperture and optimizing the collection

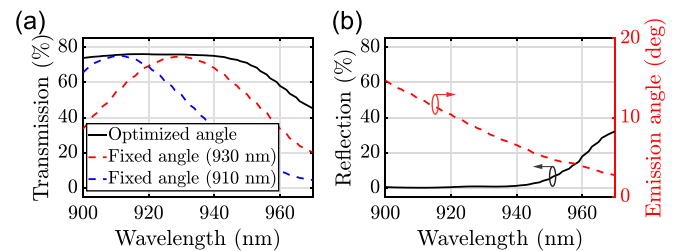


FIG. 3. (a) Simulated transmission spectrum to the Gaussian mode at 10 K, considering an adjustable collection angle optimized for each wavelength (continuous line) or fixed collection angles optimized for 930 nm (red dashed line) and 910 nm (blue dashed line), respectively. (b) Simulated reflection increases at longer wavelengths as the light emission angle reaches zero.

angle for each wavelength, the achievable collection efficiency is shown by the solid black line in Fig. 3(a). Figure 3(b) shows the intrinsic reflection and emission angles of the designed grating, which are independent of the collection scheme. At longer wavelengths, the back-reflection increases as the emission angle approaches zero (perfect vertical emission), which can be explained by the increased in-plane component of second-order diffraction back into the membrane. We also analyzed theoretically the effect of under-/over-etching of the grating grooves, which is the most sensitive parameter. Simulation shows that the transmission will drop by 3-dB at the design wavelength for an over-etching of 27 nm. The back-reflection would be further reduced in the case of under-etching, but it is quite sensitive to over-etching, increasing to 10%, 20%, and 60% for over-etching of 10 nm, 20 nm, and 30 nm, respectively.

The devices were fabricated on a 160-nm-thick GaAs membrane containing a layer of InAs QDs in the center, grown on top of a 1150-nm-thick  $\text{Al}_{0.75}\text{Ga}_{0.25}\text{As}$  sacrificial layer. The layers are grown by molecular beam epitaxy on a (100) GaAs wafer. The fabrication process consists of two electron beam lithography steps followed by dry etching. In the first step, the grating grooves are defined and etched using low-power  $\text{BCl}_3/\text{Ar}$  RIE. The shallow-etched grooves show a loading effect (RIE lag) which resulted in a size-dependent reduction of the etch rate in the grooves. In the second step, the waveguides and focusing tapers, aligned within 50 nm tolerance to the grooves, are written and deeply etched using  $\text{BCl}_3/\text{Cl}_2/\text{Ar}$  inductively coupled plasma RIE (ICP-RIE). To achieve the required alignment tolerance, Ti/Au alignment marks are patterned and lifted off beforehand. Finally, the membrane is released by etching the  $\text{Al}_{0.75}\text{Ga}_{0.25}\text{As}$  layer in a 10% solution of hydrofluoric acid followed by a residue removal procedure discussed in Ref. 2.

To measure the efficiency of the fabricated structures, we use a device consisting of two identical gratings connected by a suspended single-mode nanophotonic waveguide, shown in Fig. 4(a). The sample is mounted in a He-flow cryostat and measured at both room and cryogenic (10 K) temperatures. We illuminate one grating from free-space with a broadband laser source (SuperK EXTREME) and collect from the other via a single objective (Nikon 40X, NA = 0.6). The collected light is coupled into a fiber through a zoom-fiber collimator (Thorlab ZC618APC-B) with an adjustable focal length to match the emission beam size and sent to a spectrometer. The in- and out-coupling angles from the gratings and the focal length of the fiber collimator are manually adjusted to maximize the transmission signal  $I_{tot}$ . As a reference power for normalization,  $I_{ref}$ , we use the reflected light from the surface in a homogeneous, unpatterned part of the same sample. The normalized transmission through the whole device is given by  $T_{tot} = (I_{tot}/I_{ref})R_{\text{GaAs}}$ , where  $R_{\text{GaAs}}$  is the reflection coefficient from GaAs bulk and  $R_{\text{GaAs}} = (n_{\text{GaAs}} - 1)^2 / (n_{\text{GaAs}} + 1)^2 \approx 0.31$  for normal incidence. Neglecting the waveguide loss and assuming that the two gratings are identical, the efficiency of a single grating is  $\sqrt{T_{tot}}$ , which gives a lower bound estimation of the grating efficiency. The value of  $\sqrt{T_{tot}}$  is plotted in Figs. 4(b) and 4(d) for room and cryogenic (10 K) temperatures, respectively. The fringes at the long wavelength side of the

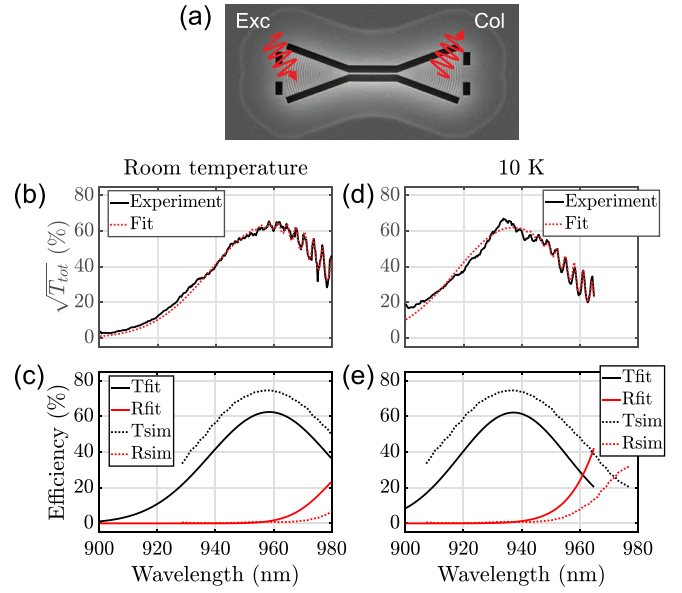


FIG. 4. (a) Nanobeam waveguide with in- and out-port gratings for characterization. Experimental and fitted transmission at (b) room temperature and (d) 10 K. The fitted  $T$  and  $R$  values are compared with simulated values at (c) room temperature and (e) 10 K with wavelength-shifted design curves.

transmission spectrum indicate back-reflection from the grating, which interferes with the forward propagating light and forms standing waves in the nanobeam waveguide. In this case, a FP cavity model is needed to extract an accurate transmission and reflection spectrum of a single grating. The cavity model of the intensity transmission through the device is given by

$$T_{tot}(\lambda) = \frac{T^2(\lambda)}{|R(\lambda)e^{i2\beta(\lambda)L} - 1|^2},$$

where  $T(\lambda)$  and  $R(\lambda)$  are the transmission and the reflection of a single grating, respectively,  $\beta(\lambda) = 2\pi n_g/\lambda$  is the propagation constant of the waveguide mode, and  $L$  is the length of the waveguide.

We fit the model to the data assuming that  $T(\lambda)$  and  $R(\lambda)$  are described by Gaussian functions, i.e.,  $T(\lambda) = T_0 e^{-((\lambda - \lambda_T)/\sigma_T)^2}$  and  $R(\lambda) = R_0 e^{-((\lambda - \lambda_R)/\sigma_R)^2}$ . The fits are shown as dotted red lines in Figs. 4(b) and 4(d), while the extracted spectra for  $T(\lambda)$  and  $R(\lambda)$  are shown in Figs. 4(c) and 4(e). The transmission spectrum with a peak  $T_0 = 62.5 \pm 0.3\%$  at a central wavelength  $\lambda_T = 958.5 \pm 0.1$  nm and a 3-dB bandwidth of  $48.5 \pm 0.6$  nm is obtained for room temperature data. At cryogenic temperatures, the transmission peak shifts to shorter wavelengths ( $\lambda_T = 937.2 \pm 0.2$  nm and  $T_0 = 62.2 \pm 0.5\%$ ) due to the reduction of the material refractive index. The 3-dB bandwidth slightly reduces to  $43.7 \pm 0.9$  nm. The back-reflection at the central wavelength is  $<1\%$  and negligible for shorter wavelengths as expected from numerical analysis. The theoretical  $T(\lambda)$  and  $R(\lambda)$  spectra are shifted to the experimental central wavelength for ease of comparison. The discrepancy between the numerical analysis and the measured data is likely due to loss in the waveguide, fabrication errors, or alignment issues.

For the application of efficient single-photon collection, we replace the shallow-etched grating at one end of the

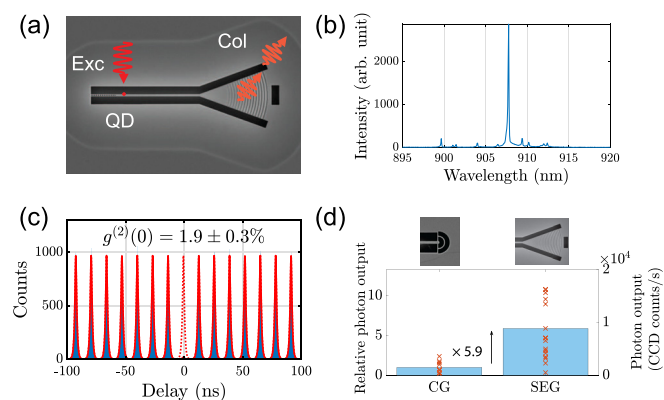


FIG. 5. (a) Single-photon source with QDs embedded in a nanobeam waveguide terminated by a photonic crystal mirror and a grating. (b) Typical QD emission spectrum. (c) Auto-correlation measurement for the QD emission line at 907.8 nm in (b). The data are fitted (red lines) to extract  $g^{(2)}(0)$ . (d) Statistic measurements of collected photon counts from devices with the circular grating (CG) and the shallow-etched grating (SEG). Photon count rates from all the QDs are marked with crosses, and bars represent the mean of the counts.

waveguide in Fig. 4(a) with a photonic crystal (PhC) mirror,<sup>25</sup> as shown in Fig. 5(a). The QDs were excited from free-space by a pulsed laser at 805 nm (above the GaAs bandgap) with a repetition rate of 76 MHz. A typical spectrum of QD emission collected from a shallow etched grating device is shown in Fig. 5(b). To validate the single-photon nature of the collected light, an auto-correlation measurement shown in Fig. 5(c) was performed on a bright emission line at 907.8 nm. The data show a rather low multi-photon emission probability of  $g_2(0) = 1.9 \pm 0.3\%$  at zero time delay, indicating a high-level of pure single-photon emission from the device.

Since circular gratings are commonly used for out-coupling of single-photons in a suspended GaAs platform,<sup>3,9,16–18</sup> it would be interesting to compare the photon collection efficiency from shallow-etched gratings to circular gratings. To quantify statistically the collection efficiency improvement, we measured on 10 and 15 QDs from devices with circular gratings and shallow-etched gratings on the same chip, respectively. As shown in Fig. 5(d), photon count rates from emitters (at saturation) coupled to shallow-etched gratings are on average 5.9 times larger to those coupled to circular gratings, in good agreement with the transmission measurements. The collected count-rate value from different QDs or devices has a large variation, which can be attributed to various reasons, such as the position-dependence of the QD emission efficiency in nanostructures<sup>20</sup> and blinking due to the unstable charge environment in the vicinity of the QD.<sup>22,26</sup> With the designed grating, the highest single-photon rate we measured is 1.3 MHz in the optical fiber (corrected to the spatial filter efficiency of 0.7 and an avalanche photodiode efficiency of 0.32).

To conclude, we have shown a shallow-etched grating coupler on a GaAs membrane system for highly efficient out-of-plane fiber coupling. Using a 3D FDTD solver, the gratings are optimized to give 74.6% transmission to the fiber and a greatly reduced back-reflection of 0.85%. We have experimentally measured >60% coupling efficiency with a 3-dB bandwidth of >43 nm and <1% reflection on the fabricated structures at both room and cryogenic temperatures, making

the designed gratings promising for high performance classical and quantum photonic circuits. As an example, we show that the single-photon collection efficiency from embedded GaAs QDs is greatly improved using the designed grating by a factor of 6 compared to conventional circular gratings on the same chip. The proposed grating enables a fast and accurate characterization of quantum photonic devices and offers an efficient interface for on-chip quantum functional devices.

The authors gratefully acknowledge Rüdiger Schott, Andreas D. Wieck, and Arne Ludwig for growing the GaAs wafers with quantum dots and Tommaso Pregonato for assistance in fabrication. We gratefully acknowledge financial support from the Danish National Research Foundation (Center of Excellence “Hy-Q”), the Europe Research Council (ERC Advanced Grant “SCALE”), Innovation Fund Denmark (Quantum Innovation Center “Qubiz”), the Danish Research Infrastructure Grant (QUANTECH), and the Danish Council for Independent Research (grant number 4184-00203).

<sup>1</sup>C. P. Dietrich, A. Fiore, M. G. Thompson, M. Kamp, and S. Höfling, “GaAs integrated quantum photonics: Towards compact and multi-functional quantum photonic integrated circuits,” *Laser Photonics Rev.* **10**, 870–894 (2016).

<sup>2</sup>L. Midolo, T. Pregonato, G. Kiršanskė, and S. Stobbe, “Soft-mask fabrication of gallium arsenide nanomembranes for integrated quantum photonics,” *Nanotechnology* **26**, 484002 (2015).

<sup>3</sup>M. Arcari, I. Söllner, A. Javadi, S. L. Hansen, S. Mahmoodian, J. Liu, H. Thyrestrup, E. H. Lee, J. D. Song, S. Stobbe *et al.*, “Near-unity coupling efficiency of a quantum emitter to a photonic crystal waveguide,” *Phys. Rev. Lett.* **113**, 093603 (2014).

<sup>4</sup>D. Englund, A. Faraon, I. Fushman, N. Stoltz, P. Petroff, and J. Vučković, “Controlling cavity reflectivity with a single quantum dot,” *Nature* **450**, 857 (2007).

<sup>5</sup>T. Lund-Hansen, S. Stobbe, B. Julsgaard, H. Thyrestrup, T. Sünner, M. Kamp, A. Forchel, and P. Lodahl, “Experimental realization of highly efficient broadband coupling of single quantum dots to a photonic crystal waveguide,” *Phys. Rev. Lett.* **101**, 113903 (2008).

<sup>6</sup>T. Ba Hoang, J. Beetz, L. Midolo, M. Skacel, M. Lermer, M. Kamp, S. Höfling, L. Balaet, N. Chauvin, and A. Fiore, “Enhanced spontaneous emission from quantum dots in short photonic crystal waveguides,” *Appl. Phys. Lett.* **100**, 061122 (2012).

<sup>7</sup>H. Thyrestrup, G. Kiršanskė, H. Le Jeannic, T. Pregonato, L. Zhai, L. Raahauge, L. Midolo, N. Rotenberg, A. Javadi, R. Schott *et al.*, “Quantum optics with near-lifetime-limited quantum-dot transitions in a nanophotonic waveguide,” *Nano Lett.* **18**, 1801–1806 (2018).

<sup>8</sup>J. Shin, Y.-C. Chang, and N. Dagli, “0.3 V drive voltage GaAs/AlGaAs substrate removed Mach-Zehnder intensity modulators,” *Appl. Phys. Lett.* **92**, 201103 (2008).

<sup>9</sup>I. Luxmoore, N. Wasley, A. Ramsay, A. Thijssen, R. Oulton, M. Hugues, A. Fox, and M. Skolnick, “Optical control of the emission direction of a quantum dot,” *Appl. Phys. Lett.* **103**, 241102 (2013).

<sup>10</sup>C. Bentham, I. Itskevich, R. Coles, B. Royall, E. Clarke, J. O’Hara, N. Prtljaga, A. Fox, M. Skolnick, and L. Wilson, “On-chip electrically controlled routing of photons from a single quantum dot,” *Appl. Phys. Lett.* **106**, 221101 (2015).

<sup>11</sup>L. Midolo, S. L. Hansen, W. Zhang, C. Papon, R. Schott, A. Ludwig, A. D. Wieck, P. Lodahl, and S. Stobbe, “Electro-optic routing of photons from a single quantum dot in photonic integrated circuits,” *Opt. Express* **25**, 33514–33526 (2017).

<sup>12</sup>Q. V. Tran, S. Combré, P. Colman, and A. De Rossi, “Photonic crystal membrane waveguides with low insertion losses,” *Appl. Phys. Lett.* **95**, 061105 (2009).

<sup>13</sup>M. Davanço, M. T. Rakher, W. Wegscheider, D. Schuh, A. Badolato, and K. Srinivasan, “Efficient quantum dot single photon extraction into an optical fiber using a nanophotonic directional coupler,” *Appl. Phys. Lett.* **99**, 121101 (2011).

<sup>14</sup>C.-M. Lee, H.-J. Lim, C. Schneider, S. Maier, S. Höfling, M. Kamp, and Y.-H. Lee, “Efficient single photon source based on  $\mu$ -fibre-coupled tunable microcavity,” *Sci. Rep.* **5**, 14309 (2015).

- <sup>15</sup>R. S. Daveau, K. C. Balram, T. Pregolato, J. Liu, E. H. Lee, J. D. Song, V. Verma, R. Mirin, S. W. Nam, L. Midolo *et al.*, “Efficient fiber-coupled single-photon source based on quantum dots in a photonic-crystal waveguide,” *Optica* **4**, 178–184 (2017).
- <sup>16</sup>A. Faraon, I. Fushman, D. Englund, N. Stoltz, P. Petroff, and J. Vučković, “Dipole induced transparency in waveguide coupled photonic crystal cavities,” *Opt. Express* **16**, 12154–12162 (2008).
- <sup>17</sup>R. Coles, D. Price, J. Dixon, B. Royall, E. Clarke, P. Kok, M. Skolnick, A. Fox, and M. Makhonin, “Chirality of nanophotonic waveguide with embedded quantum emitter for unidirectional spin transfer,” *Nat. Commun.* **7**, 11183 (2016).
- <sup>18</sup>Z. Bishop, A. Foster, B. Royall, C. Bentham, E. Clarke, M. Skolnick, and L. Wilson, “Electro-mechanical control of an on-chip optical beam splitter containing an embedded quantum emitter,” *Opt. Lett.* **43**, 2142–2145 (2018).
- <sup>19</sup>G. Roelkens, D. Vermeulen, F. Van Laere, S. Selvaraja, S. Scheerlinck, D. Taillaert, W. Bogaerts, P. Dumon, D. Van Thourhout, and R. Baets, “Bridging the gap between nanophotonic waveguide circuits and single mode optical fibers using diffractive grating structures,” *J. Nanosci. Nanotechnol.* **10**, 1551–1562 (2010).
- <sup>20</sup>G. Kiršanskė, H. Thyrrerstrup, R. S. Daveau, C. L. Dreeßen, T. Pregolato, L. Midolo, P. Tighineanu, A. Javadi, S. Stobbe, R. Schott *et al.*, “Indistinguishable and efficient single photons from a quantum dot in a planar nanobeam waveguide,” *Phys. Rev. B* **96**, 165306 (2017).
- <sup>21</sup>L. Chrostowski and M. Hochberg, *Silicon Photonics Design: From Devices to Systems* (Cambridge University Press, 2015).
- <sup>22</sup>P. Lodahl, S. Mahmoodian, and S. Stobbe, “Interfacing single photons and single quantum dots with photonic nanostructures,” *Rev. Mod. Phys.* **87**, 347 (2015).
- <sup>23</sup>See <https://www.lumerical.com/tcad-products/fdtd/> for information on simulation software.
- <sup>24</sup>H. Jansen, M. de Boer, R. Wiergerink, N. Tas, E. Smulders, C. Neagu, and M. Elwenspoek, “BSM 7: RIE lag in high aspect ratio trench etching of silicon,” *Microelectron. Eng.* **35**, 45–50 (1997).
- <sup>25</sup>C. Sauvan, G. Lecamp, P. Lalanne, and J.-P. Hugonin, “Modal-reflectivity enhancement by geometry tuning in photonic crystal microcavities,” *Opt. Express* **13**, 245–255 (2005).
- <sup>26</sup>J. Liu, K. Konthasinghe, M. Davanço, J. Lawall, V. Anant, V. Verma, R. Mirin, S. W. Nam, J. D. Song, B. Ma, Z. S. Chen, H. Q. Ni, Z. C. Niu, and K. Srinivasan, “Single self-assembled InAs/GaAs quantum dots in photonic nanostructures: The role of nanofabrication,” *Phys. Rev. Appl.* **9**, 064019 (2018).